Optics & Laser Technology 56 (2014) 343–347

Contents lists available at ScienceDirect

Optics & Laser Technology

journal homepage: www.elsevier.com/locate/optlastec

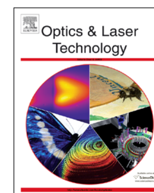

Improved performances of 850 nm vertical cavity surface emitting lasers utilizing the self-planar mesa structure

Jianwei Zhang, Yongqiang Ning *, Xing Zhang, Yugang Zeng, Jian Zhang, Lijun Wang

State Key Laboratory of Luminescence and Application, Changchun Institute of Optics, Fine Mechanics and Physics, Chinese Academy of Sciences, 3888 Southeast Lake Road, Changchun 130033, PR China

ARTICLE INFO

Article history:
Received 16 April 2013
Received in revised form
2 September 2013
Accepted 6 September 2013
Available online 8 October 2013

Keywords:
VCSELs
Self-planar mesa
Thermal analysis

ABSTRACT

We presented the self-planar mesa structure for improving the performances of 850-nm oxide-confined vertical cavity surface emitting lasers (VCSELs). By employing the self-planar mesa, the maximum output power was increased from 8 mW to more than 11 mW, and the maximum wall–plug efficiency was improved from 26% to 36% for the VCSEL with an oxide aperture size of 13 μm at 15 °C. The thermal resistance was decreased from 1.16 °C/mW to 0.94 °C/mW. Thermal simulations about different mesa structures were carried out. And the enhanced lateral heat dissipation and current diffusion within VCSELs was considered to be the main reason for improved performances.

Crown Copyright © 2013 Published by Elsevier Ltd. All rights reserved.

1. Introduction

VCSELs are the most miniature and economically efficient laser emitters developed so far. The unique geometry of VCSELs results in several significant advantages over their edge-emitting counterparts, including low power consumption, longitudinal single-mode operation [1–3]. However, the device performance such as optical output power, wall plug efficiency is always limited by self-heating effects [3–7]. For the top emitting VCSEL, the self-heating effect is more serious due to the low conductance and high optical absorption of P-DBR structure. Thus it is essential to apply effective thermal management and reduce the series resistance of VCSELs for less heat generation.

Previously, the bandgap and doping profiles of hetero-interfaces within VCSELs were always investigated, aiming at improving its conductivity [8,9]. Presently, much effort had been made to improve the heat dissipation by optimizing the processing structure of VCSELs [10–14]. The intracavity-contacted VCSEL structure was developed to eliminate the self heating of DBR [10]. And the enhanced heat dissipation was proved by employing the asymmetric intracavity-contacted VCSEL [11]. Recently, top emitting VCSELs with a self-aligned top contact and evaporated gold or plated copper heatsink were reported [12,13]. In a more recent work, the elongated shape of emission area was proposed to improve the heat dissipation and carrier-transport in top emitting VCSELs [14]. The rectangular shaped VCSELs exhibited improved thermal performances due to better heat and carrier transport.

In this paper, we report on a self-planar mesa structure to enhance the lateral heat dissipation of VCSELs. Thermal analysis of this structure was carried out by COMSOL multiphysics software. Without a conventional planar process, the simple fabrication process of this structure lead to low manufacturing cost and good reproducibility of devices. Improved performances of VCSELs were gained from experimental results.

2. Fabrication

The self-planar mesa structure was fabricated from a metal–organic chemical vapor deposition grown 850-nm VCSEL on an n-type substrate. The carbon-doped p-type Bragg reflector consisted of 22 pairs of $Al_{0.12}Ga_{0.88}As/Al_{0.9}Ga_{0.1}As$ layers. The active region was composed of three 6-nm-thick GaAs quantum wells for an emission wavelength of about 835 nm. For selective oxidation, a 30-nm-thick $Al_{0.98}Ga_{0.02}As$ layer was partially used instead of the $Al_{0.9}Ga_{0.1}As$ layer, near the active region, in the p-side DBR. The 33-period n-mirror below the active region was Si-doped. Schematic illustration of a self-planar mesa structure is shown in Fig. 1.

The microscopic image from top view of a final VCSEL device with the self-planar mesa is shown in Fig. 2(a). Fig. 2(b) shows a sample after $Al_{0.98}Ga_{0.02}As$ layer oxidization and removing top DBR during the fabrication process. An oxide aperture of nearly diamond shape as a color of light white could be seen at the center of the circle part of mesa structure.

* Corresponding author. Tel./fax: +86 431 86176348.
E-mail address: zcjw1985@126.com (Y. Ning).

0030-3992/$ - see front matter Crown Copyright © 2013 Published by Elsevier Ltd. All rights reserved.
http://dx.doi.org/10.1016/j.optlastec.2013.09.005

The fabrication procedures were as follows. First, the self planar mesa was formed by lithography and unselective wet-etching as shown in Fig. 1. The solution used for the wet-etching is H_3PO_4:H_2O_2:H_2O = 1:1:3. The mesa included three parts: the circular portion with a diameter of 60 μm was lasers' main body; the square portion with a diameter of about 70 μm × 80 μm was used for bond pad mesa, and the triangular region served as a bridge to connect these two portions and to form a conjunct plane.

Then, the oxide aperture was formed by wet oxidization in the circular portion (Fig. 1) with oxidization condition of at 420 °C under 30 sccm N_2 gas bubbled through 90 °C deionized water. The oxide aperture showed a nearly diamond shape, with the diagonal length of 11–13 μm in Fig. 2(b). This was caused by the oxidization rate difference between the neck of mesa and the exposed mesa side. The oxidization reaction firstly occurred at the exposed $Al_{0.98}Ga_{0.02}As$ layer, and then diffused into the inner part, thus the neck of mesa would suffer a slower oxidization rate. Due to this, a small dip appeared at the oxidation aperture facing the direction of the neck.

After oxidization, SiO_2 insulating layer was deposited onto the mesa, and then partially etched for the annular metal contact electrode formation. Then the Ti/Au was evaporated on the p-contact layer. The lithography and lift-off processes were carried out to form the light emission window, as shown in Fig. 2(a). Finally, the n-type contact metal (Au/Ge/Ni) was deposited on to the bottom side of the wafer after substrate thinning, and conventional metal electrodes annealing was carried out. In the above fabrication procedures, conventional BCB planar processes were avoided due to the induced conjunct plane of self-planar mesa. Thus the above process could lower manufacturing costs.

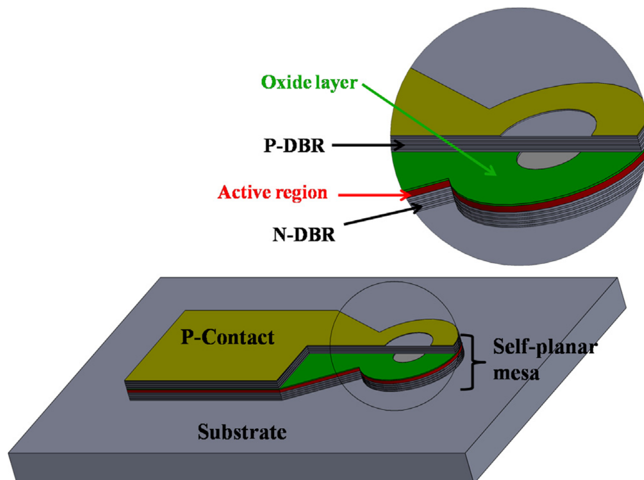

Fig. 1. Schematic illustration of a self-planar mesa structure, with the partial cross-sectional view of the VCSEL structure shown in the inserted figure.

After VCSEL fabrication, the separated device chips were cleaved and mounted on the heatsinks. Light output power and voltage characteristics under continuous-wave (CW) operation of VCSEL devices were tested by a Keithley lasers *L*–*I*–*V* test system. The lasing wavelength was measured by an OceanOptics USB4000-VIS-NIR fiber spectrometer.

3. Measurements

Fig. 3(a) compares the continuous-wave (CW) light output versus current (*L*–*I*) and voltage (*V*) characteristics of two VCSELs with different mesa structures at 15 °C. Both had identical mesa and oxide aperture diameters of 60 μm and 13 μm, respectively. The wall plug efficiency versus current is also shown in Fig. 3(b).

In Fig. 3(a), the threshold current of 1.4 mA for the self-planar mesa VCSEL was slightly lower than that of 1.8 mA for the circle mesa one. The slope of the power curve was similar for both devices, but the self-planar mesa VCSEL showed higher rollover current and maximum output power. The maximum output power was 11.15 mW for the self-planar mesa VCSEL and 8.11 mW for the circle one. In addition, the differential resistance of the self-planar mesa VCSEL was also much lower than that of the circle mesa. The low differential resistance was believed to be due to the large current spreading area under the active region along with consequently formed much lower n-DBR resistance and substrate resistance.

As the injection current increased, the increased device temperatures caused the rapid decrease of internal quantum efficiency, and this was responsible for the onset of thermal rollover [10]. As shown in Fig. 3(a), the self-planar mesa structure supported higher rollover current and maximum output power.

As shown in Fig. 3(b), the maximum wall plug efficiency was improved from 26% to 36% by utilizing the self-planar mesa structure. The maximum wall plug efficiency appeared when the injection current was about three times of threshold current. Then the wall plug efficiency decreased due to the self-heating inducing internal quantum efficiency degeneration [10]. For the self-planar mesa VCSEL, the wall–plug efficiency decreased gradually after the maximum value was reached, while for the circle mesa device, it decreased much rapidly due to the severe self-heating. Thus the proposed self-planar mesa structure was demonstrated effective in improving the operating performances of VCSEL.

Fig. 4 shows measured lasing wavelengths as a function of the injection current for the device with the oxide aperture of 13 μm. The red-shift of wavelength with increasing injection current was evident in the figure. Self-heating changed the temperature-

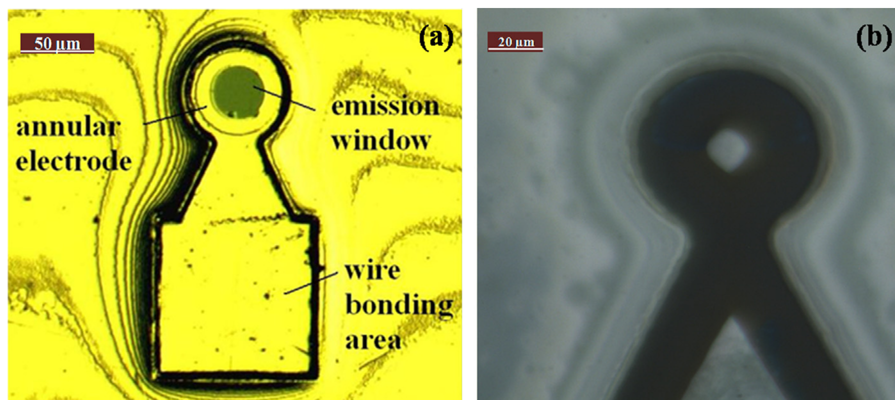

Fig. 2. Microscopic images from top view: (a) a final self-planar mesa VCSEL device; and (b) the sample after $Al_{0.98}Ga_{0.02}As$ layer oxidization and removing top DBR stacks.

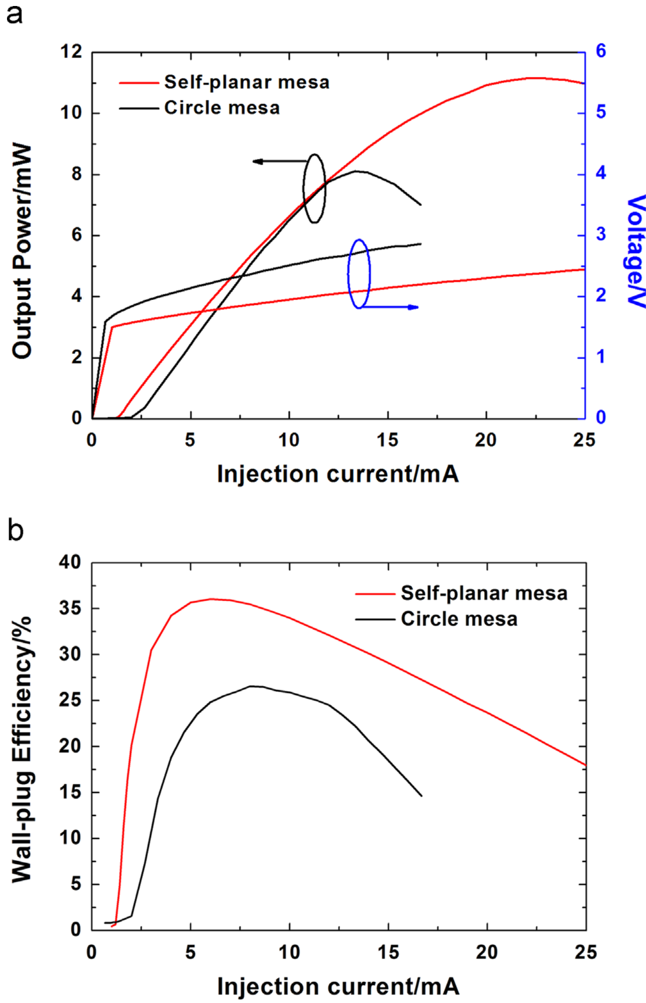

Fig. 3. Measured static *L–I–V* characteristics (a) and wall plug efficiency (b) at 15 °C of a 850-nm VCSEL with a 13 μm oxide-aperture diameter. Red lines denote the self-planar mesa VCSEL and dark lines correspond to the circle mesa VCSEL. (For interpretation of the references to color in this figure legend, the reader is referred to the web version of this article.)

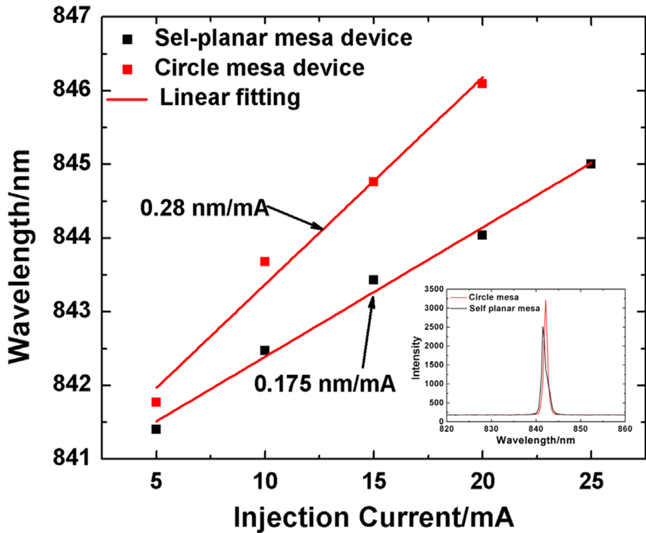

Fig. 4. Measured lasing wavelength of VCSELs with two different mesa structures plotted as a function of the bias current. The oxide aperture radius was 13 μm. Inserted was the lasing wavelength of different mesa devices at 5 mA injection current.

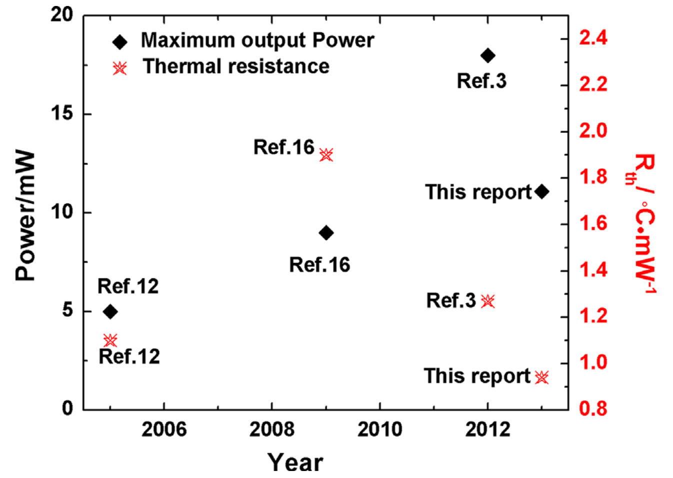

Fig. 5. The reported maximum output power and thermal resistance of 850 nm VCSELs in this letter and its comparison to the best results from the literature. The black box represented the maximum output power, while the red triangle represented the thermal resistance. (For interpretation of the references to color in this figure legend, the reader is referred to the web version of this article.)

dependent refractive indices of materials, and hence caused corresponding change of the resonant wavelength. Obviously, the self-heating effect was more serious in the circle mesa device than the self-planar mesa device due to its more rapid red shift of wavelength. Using $\Delta\lambda/\Delta T = 0.07\ \text{nm}/^{\circ}C$ [12], thermal resistances ($R_{th} = \Delta T/\Delta(P_e) = \Delta\lambda/\Delta(P_e)/\Delta\lambda/\Delta T$) of VCSEL devices were determined by measuring the wavelength dependence of the laser spectra as a function of the electrical input power. ΔT was the temperature rise, and ΔP_e was the change of electrical input power [15]. From the measured parameters, the corresponding thermal resistance is 1.16 °C/mW for the circle mesa device, while 0.94 °C/mW for the self-planar mesa device. Thus the R_{th} was reduced by 18% due to the enhanced lateral thermal dissipation by the self-planar mesa structure. The 0.94 °C/mW thermal resistance reported in this letter was rather lower than that reported in previous publications.

Fig. 5 summarizes several good results of 850 nm VCSELs that were fabricated using various techniques and comparison to our report. Improvements in the maximum output power and thermal resistance of 850 nm VCSELs were gained in our report. The maximum output power in this report was lower than Ref. [3], but higher than in Refs. [12,16]. Higher maximum output power in Ref. [3] was partially due to its larger oxidation aperture of 14 μm than that of 13 μm in this letter. The thermal resistance reported in this letter (0.94 °C/mW) was lower than other three literatures (1.1 °C/mW, 1.9 °C/mW, 1.27 °C/mW) in Fig. 5. Thus the self-planar mesa structure could improve the heat dissipation within VCSEL devices efficiently.

4. Thermal simulation and discussion

Thermal analysis based on the electrical-thermal coupling model was conducted to model the heat transport in the VCSEL structure using the commercial COMSOL software. The heat source P_{ht} was mainly distributed in the active region, calculated from a reliable empirical model [17] as follows:

$$P_{ht} = \frac{1}{q}E_B(T)I_b - \frac{1}{q}\cdot E_L(T)\eta_d(T)(I_b - I_{\text{th}}) + \frac{dV}{dI}I_b^2, \quad (1)$$

$E_B(T)$, $E_L(T)$ and $\eta_d(T)$ are the temperature-dependent barrier bandgap energy, quantum well bandgap energy and slope efficiency of VCSEL, respectively. I_b is the injected current, I_{th} is the

Table 1
Basic material parameters of 850 nm VCSEL used for the simulation.

Layer	Material	Thermal conductivity (W/m K)	Electric conductivity (S/m)
P-contact metal	TiPtAu	315	6.3e7
Contact layer	GaAs	44	9e5
P-DBR	$Al_{0.12}Ga_{0.88}As/Al_{0.9}Ga_{0.1}As$	$K_{\parallel}=31.2$, $K_{\perp}=27.7$	$\sigma_{\parallel}=276.1$, $\sigma_{\perp}=41$
Oxidation layer/aperture	$Al_xO_y/Al_{0.98}Ga_{0.02}As$	0.6/56.4	1e−5/1.5e3
Grading layer	$Al_{0.6}Ga_{0.4}As–Al_{0.3}Ga_{0.7}As$	17.4	681.7
Spacing layer	$Al_{0.3}Ga_{0.7}As$	11.6	1.3e4
3 MQW	$GaAs/Al_{0.3}Ga_{0.7}As$	$K_{\parallel}=32.3$, $K_{\perp}=18.6$	$\sigma_{\parallel}=590$, $\sigma_{\perp}=120$
Spacing layer	$Al_{0.3}Ga_{0.7}As$	11.6	1.3e4
Grading layer	$Al_{0.6}Ga_{0.4}As–Al_{0.3}Ga_{0.7}As$	17.4	681.7
N-DBR	$Al_{0.12}Ga_{0.88}As/Al_{0.9}Ga_{0.1}As$	$K_{\parallel}=31.2$, $K_{\perp}=27.7$	$\sigma_{\parallel}=5.9e3$, $\sigma_{\perp}=919.3$
Substrate	GaAs	44	4.5e4
N-contact metal	AuGeNi	315	6.3e7

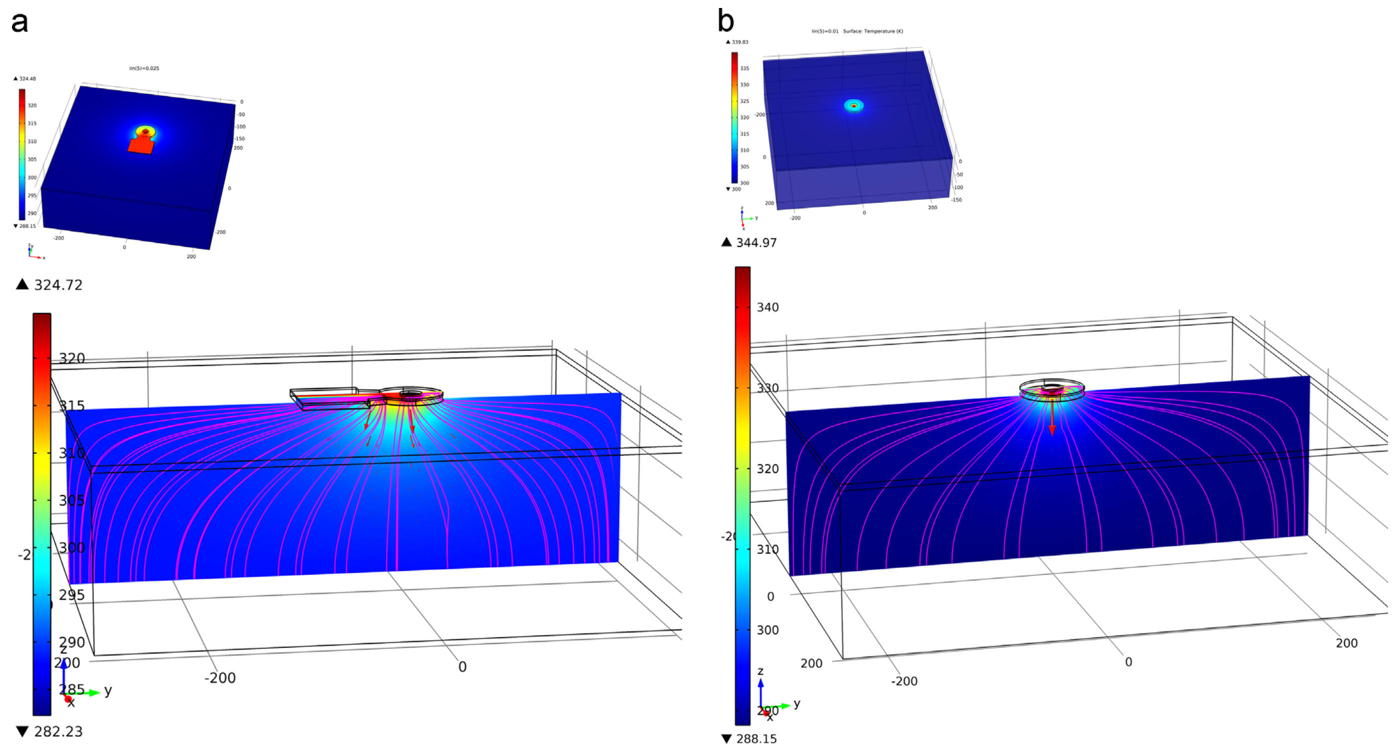

Fig. 6. Temperature, heat flux and electric current distributions in cross-sections of the self-planar mesa VCSEL (a) and circle mesa VCSEL(b), pink lines represent the heat flux and red arrows represents the electric current. (For interpretation of the references to color in this figure legend, the reader is referred to the web version of this article.)

threshold current, q is the electron charge, dV/dI represents the differential resistance of different layers.

Basic parameters used in the simulation were gained from initial measurements of an 850 nm VCSEL at room temperature. The effective thermal conductivity and electrical conductivity were taken into account in the DBR and QW region [11,18,19]. Table 1 shows the material parameters used for the simulation.

Fig. 6 shows the heat flux, electric current and temperature distribution in cross-sections of VCSELs with different mesa structures at the injection current of 8 mA. The oxidation aperture of samples used in the simulation was 13 μm, and the circle part of mesa dimension was 60 μm. The temperature of heat sink was set at 15 °C. Large amounts of heat flowed radially toward the substrate from heat sources by conduction because the device was contacted with copper heatsink through the GaAs substrate. As shown in Fig. 6(a), the heat flux was denser and spread out over a wider mesa area in the self-planar mesa structure than the circle one. The dense heat flux indicated rapid heat dissipation. Due to the larger thermal conductivity in lateral directions of VCSELs [6,11], the wider mesa area enhanced the dissipation rate of heat source. Thus it was expected that the self-planar mesa structure could efficiently reduce the thermal accumulation within VCSELs. This had been proved by the measurements in Fig. 3.

In addition to the improvement in thermal properties, the increased mesa area also significantly decreased the series resistance of VCSEL. The injection current mainly concentrated in the central part of oxide apertures in Fig. 6, however, the lateral current diffusion appeared in the N-DBR and substrate in Fig. 6(a). As the series resistance was inversely proportional to the current diffusion area, reduced series resistance could be gained by employing the self-planar mesa. Fig. 7 shows the current distribution in lateral direction of the first layer in N-DBR at the injection current of 5 mA and 10 mA.

Sharp peaks were observed on the curves of current density distribution at the position of mesa edge in Fig. 7. This was caused by the current crowding effect at the corner of mesa structure. As shown in Fig. 7, distribution of the diffusion current of circle mesa device was symmetrical at both sides of N-DBR layer under

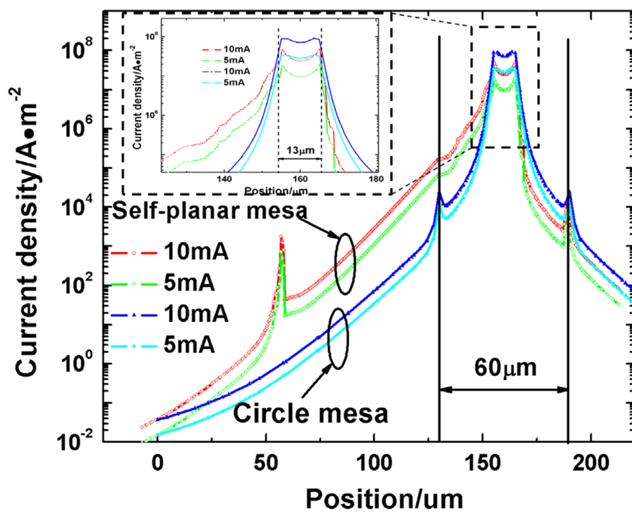

Fig. 7. Current distributions in lateral direction of the first layer of N-DBR at the injected current of 5 mA and 10 mA. The oxide aperture of VCSEL devices was 13 μm. Details of the current distribution in the area under active region were also shown in the inserted figure.

the active region, while large amount of current diffused along the square portion of the self-planar mesa. The current density outside the circle part of self-planar mesa device was larger than that of circle mesa device, while lower in the area under the active region (the inserted figure in Fig. 7). Thus, for the self-planar mesa VCSEL, the enhanced lateral current diffusion could be gained. Enhanced current diffusion in the lateral direction in N-DBR of the self-planar mesa decreased the resistance of N-DBR, thus the differential resistance of VCSEL was decreased. This could be observed in the measured *IV* curve in Fig. 3(a). As a result of the decreased resistance of N-DBR, the wall–plug efficiency of VCSEL was improved from 26% to 36% in Fig. 3(b).

5. Conclusions

In summary, we have successfully improved VCSEL performances by employing the self-planar mesa structure. The maximum output power of more than 11 mW and maximum wall–plug efficiency of 36% were gained for the VCSEL with an oxide aperture size of 13 μm at room temperature. The corresponding thermal resistance was 0.94 °C/mW. We showed that the improved performance is based on two effects. Firstly, the lateral heat dissipation was enhanced. Therefore the VCSEL have a reduced internal temperature of the active region, a smaller decrease rate of internal quantum efficiency. The second, the current diffused along a larger dimension in the N-DBR and substrate. And the decreased series resistance generated less heat.

References

[1] Iga K. Surface-emitting laser—its birth and generation of new optoelectronics field. IEEE Journal of Selected Topics in Quantum Electronics 2000;6:1201–15.

[2] Ding K, Ning CZ. Metallic subwavelength-cavity semiconductor nanolasers. Light: Science & Applications 2012;1:1–8.

[3] Baveja PP, Kögel B, Westbergh P, Gustavsson JS, Haglund Å, Maywar DN, et al. Impact of device parameters on thermal performance of high-speed oxide-confined 850-nm VCSELs. Journal of Quantum Electronics 2012;48:17–26.

[4] Donghan Wei, Shuang Du, Ting Gao, Yong Pang, Bo Zhao, Hui Li, et al. Thermal characteristic analysis of new structure in 850 nm VCSEL. In: Proceedings of the 2012 international conference on IEEE optoelectronics and microelectronics (ICOM); 2012: p. 64–7.

[5] AL-Omari AN, Alias MS, Ababneh A, Lear KL. Improved performance of top-emitting oxide-confined polyimide-planarized 980 nm VCSELs with copper-plated heat sinks. Journal of Physics D: Applied Physics 2012;45:505101-1–8.

[6] Lifeng Hou, Yongfeng Ma, Yuan Feng. Fabrication and testing of 980 nm high-power VCSEL with AlN film passivation layer. In: Proceedings of the 2012 international conference on IEEE optoelectronics and microelectronics (ICOM); 2012: p. 45–8.

[7] Wipiejewski T, Young DB, Peters MG, Thibeault BJ, Coldren LA. Improved performance of vertical-cavity surface-emitting laser diodes with Au-plated heat spreading layer. Electronics Letters 1995;31:279–81.

[8] Kojima K, Morgan RA, Mullaly T, Guth GD, Focht MW, Leibenguth RE, et al. Reduction of p-doped mirror electrical resistance of GaAs/AlGaAs vertical-cavity surface-emitting lasers by delta doping. Electronics Letters 1993;29: 1771–2.

[9] Peters MG, Thibeault BJ, Young DB, Scott JW, Peters FH, Gossard AC, et al. Band-gap engineered digital alloy interfaces for lower resistance vertical-cavity surface-emitting lasers. Applied Physics Letters 1993;63:3411–3.

[10] Scott JW, Thibeault BJ, Young DB, Coldren LA, Peters FH. High efficiency submilliamp vertical cavity lasers with intracavity contacts. IEEE Photonics Technology Letters 1994;6:678–80.

[11] Lee HK, Song YM, Lee YT, Yu JS. Thermal analysis of asymmetric intracavity-contacted oxide-aperture VCSELs for efficient heat dissipation. Solid-State Electronics 2009;53:1086–91.

[12] AL-Omari AN, Lear. KL. VCSELs with a self-aligned contact and copper-plated heatsink. IEEE Photonics Technology Letters 2005;17:1767–9.

[13] AL-Omari AN, Carey GP, Hallstein S, Watson JP, Dang G, Lear. KL. Low thermal resistance high-speed top-emitting 980-nm VCSELs. IEEE Photonics Technology Letters 2006;18:1225–7.

[14] Gronenborn S, Pollmann-Retsch J, Pekarski P, Miller M, Strösser M, Kolb J, et al. High-power VCSELs with a rectangular aperture. Applied Physics B 2011;105: 783.

[15] Dang G, Luo B, Ren F, Hobson WS, Lopata J, Pearton SJ, et al. Temperature characteristics of 850 nm, intra-cavity contacted, shallow implant-apertured vertical-cavity surface-emitting lasers. Solid-State Electronics 2002;46: 1247–9.

[16] Westbergh Petter, Gustavsson Johan S, Haglund Asa, Sk̈old Mats, Joel Andrew, Larsson Anders. High-speed, low-current–density 850 nm VCSELs. Journal of Selected Topics in Quantum Electronics 2009;15:694–702.

[17] Baveja PP, Kögel B, Westbergh P, Gustavsson JS, Haglund Å, Maywar DN, et al. Assessment of VCSEL thermal rollover mechanisms from measurements and empirical modeling. Optics Express 2011;19:15490–505.

[18] Wang JH, Savidis I, Friedman EG. Thermal analysis of oxide-confined VCSEL arrays. Microelectronics Journal 2011;42:820–5.

[19] Angelos Craig, Hinckley Steven, Michalzik Rainer, Voignier Vincent. Simulation of current spreading in bottom-emitting vertical cavity surface emitting lasers for high power operation. Proceedings of SPIE 2004;5277:261–72.